Journal of Applied Polymer Science

Reinforcement in the mechanical properties of shape memory liquid crystalline epoxy composites

Huilong Guo,[1,2] Yinwen Li,[1,2] Jian Zheng,[1,2] Jianqun Gan,[1,2] Liyan Liang,[1] Kun Wu,[1] Mangeng Lu[1]

[1]Key Laboratory of Cellulose and Lignocellulosics Chemistry, Chinese Academy of Sciences; Guangzhou Institute of Chemistry, Chinese Academy of Sciences, Guangzhou 510650, People's Republic of China

[2]University of Chinese Academy of Sciences, Beijing 100049, People's Republic of China

Correspondence to: M. Lu (E-mail: mglu@gic.ac.cn)

ABSTRACT: In this work, novel thermoresponsive shape memory composites based on glass fiber and nanosilica-modified liquid crystalline epoxies (LCEs) with lateral substituent were prepared and characterized. According to the comprehensive analysis of polarized optical microscopy, wide-angle X-ray diffraction measurements, and tan δ data, the orientation of mesogen units were hindered by the introduction of nanosilica and lateral substituents of liquid crystalline epoxies, so that additional physical cross-links except for similar chemical cross-links emerged with the introduction of surface-treated nanosilica. And the increased cross-links could enhance the shape memory properties of the composites which could recover to their original state quickly in a time shorter than 30 s with high shape fixing ratios (>96%) and high shape recovery ratios (>98%), which indicated the composites could be applied into self-deployable structural materials. Moreover, the reinforcement in the dynamic storage moduli, tensile modulus, and the tensile strength and shape memory properties indicated that glass fiber and nanosilica-modified shape memory liquid crystalline epoxy composites could be high-performance composites and could be used as new candidates for aerospace smart materials. © 2015 Wiley Periodicals, Inc. J. Appl. Polym. Sci. **2015**, *132*, 42616.

KEYWORDS: fibers; liquid crystals; mechanical properties; resins; stimuli-sensitive polymers

Received 8 February 2015; accepted 14 June 2015
DOI: 10.1002/app.42616

INTRODUCTION

Shape memory polymers (SMPs) possess the distinct ability of changing their shapes from a temporary state to their original or permanent shape after being exposed to the external stimulus such as heat, pH, light, magnetic field, and electric field. Among various stimuli-responsive SMPs, thermoresponsive SMPs arouse tremendous attention in view of their numerous applications.[1–3]

Shape memory epoxies, as the chemically cross-linked shape memory polymers, have so many desirable characteristics, such as good mechanical properties, ease of processability, composite forming properties, and very good dimensional stability, which make shape memory epoxy polymers attractive for application in the processing of many smart engineering systems.[4,5]

Liquid crystalline epoxides (LCEs), owning oriented and chemically cross-linked structure, are superior to common epoxies in the performance of better mechanical and dielectric properties in the direction of orientation, better dimensional stability, lower coefficients of thermal expansion, increased fracture toughness, and noticeable high-temperature properties.[6,7] The oriented structure of LCEs could increase packing density of the segments, resulting in increased cross-link network density.[8,9] The increasing cross-linking density could significantly improve the shape memory properties.[10] Therefore, LCEs are especially suitable for being used as advanced shape memory composites matrix. However, there were several reported studies about the shape memory effect of epoxies[11–14] and epoxy composites[15,16] but only few works focused on the shape memory effect of liquid crystalline epoxies[17,18] and their composites.

Glass-fiber-reinforced polymer composites, due to their extraordinary mechanical performance/cost ratio, are very attractive materials for many industrial applications. The mechanical performances of glass-fiber-reinforced polymer composites can be improved by importing a small amount of nanomaterials (nanosilica, carbon nanotube, nanoclay, nanocellulose, nanothermoplastic fibers, etc.) to the polymer matrix, which is attributed to that nanomaterials can modify the intrinsic defects on the surfaces of GFs. Diego Pedrazzoli *et al.*[19] found that the interfacial adhesion between E-glass fibers and polypropylene was enhanced by dispersing various types and amounts of silica nanoparticles in the polymer matrix, leading to a remarkable enhancement of both elastic modulus and creep stability of the selected polypropylene

matrix. Manjunatha *et al.*[20] utilized the neat and the nanosilica-modified epoxy resins to fabricate glass-fiber-reinforced plastic (GFRP) composite laminates. The fatigue life and the mechanical properties of the GFRP composite were increased due to the silica nanoparticles. There were other reports which confirmed that nanoparticles homogeneously dispersed in a polymer matrix or localized at the interfacial region could enhance the interfacial adhesion between fiber and matrix, resulting in the enhancement of the mechanical properties of the polymer matrix.[21–26] Therefore, it was expected that the mechanical properties and shape memory properties would be improved with the introduction of surface-treated nanosilica to the glass-fiber-reinforced LCE.

This article deals with the preparation and characterization of a novel thermoresponsive shape memory composites based on glass fiber and nanosilica-modified LCE with lateral substituent. In this study, we report the benefits of surface-treated nanosilica on the mechanical properties and shape memory properties of the glass-fiber-reinforced LCE with lateral substituent.

EXPERIMENTAL

Materials

LCE with lateral substituent (LCE2, LCE6, LCE10) (2,5-bis [4-(glycidyl ether) benzoyloxy] benzoic acid (ethyl, *n*-hexyl, *n*-decyl ester; Figure 1) was synthesized in our laboratory according to the program proposed by our group in early reports.[27] 4,4′-Diaminodiphenylmethane (DDM; Figure 1) was purchased from Aladdin and was used as curing agent. Glass fabric (300 g/m^2 plain) was purchased from Guangzhou Hetaisi Chemical Materials Co., Ltd. and was cleaned in dichloromethane for 3 days, distilled water for 1 day, and dried in vacuum at 80°C for 2 days before using. Nanosilica (20 nm, purity 99.9%) was supplied by Shanghai Yuantai Chemical Products Co., Ltd. Nanosilica was surface treated by 1% wt silane coupling agent (KH570, supplied by Shenzhen, south China Xin Yang Technology Co., Ltd.) in acetone with ultrasonic dispersing for 30 min.

Composites Manufacturing

The stoichiometric amount of LCE and DDM was dissolved in dichloromethane, with addition of 3% wt surface-treated nanosilica which was uniformly dispersed into the mixture using an ultrasonic dispersion for 30 min, a layer of glass fabric was infiltrated by the mixed solution of nanosilica-modified LCE/DDM for 30 min. Then dichloromethane was removed under reduced pressure at room temperature, the percentage of glass fibers with respect to the matrix was 30 wt %. The samples were cured at low temperature which is the isotropic temperature of LCE/DDM mixtures, for 16 h to ensure the totally reaction of linear chain extension and postcured at 160°C for 6 h, 200°C for 1 h to guarantee completely branching and cross-linking. After curing, the cured product (referred to LCE/DDM/GF/SiO_2, abbreviated as LCE/GF/SiO_2 in the figure legend and table sample name) was extracted from the mold and to be tested. LCE6/DDM (abbreviated as LCE6 in the figure legend and table sample name) resin and LCE6/DDM/GF (abbreviated as LCE6/GF in the figure legend and table sample name) composite were manufactured through the same curing process, in order to be compared with the nanosilica-modified LCE/DDM/GF composites.

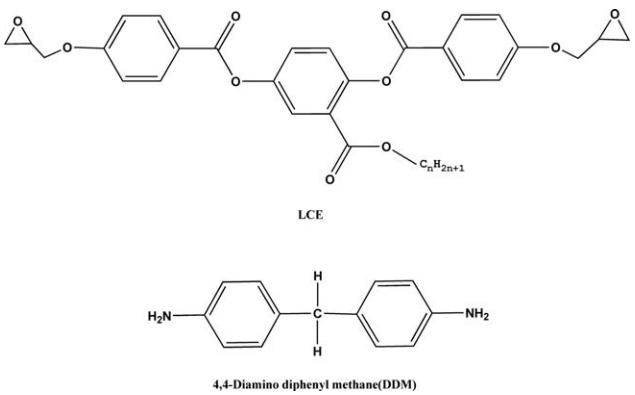

Figure 1. Chemical structures of LCE and DDM.

Physical Measurements

The liquid crystalline phase structure of LCE with lateral substituents and their composites was examined by a polarized light optical microscopy (POM) (Orthoglan, LEITZ, Germany) and wide-angle X-ray diffraction measurements (WAXS) which were carried out with a Rigaku Diffractometer (D/MAX-1200), using monochromatic Cu Karadiation (40 kV, 30 mA) and secondary graphite monochromator, with the X-ray scatting intensities being detected by a scintillation counter incorporating a pulse-height analyzer.

The tensile test at room temperature and 150°C were carried out by an Instron mechanical testing machine (SHT5000, Shenzhen SANS Testing Machine). The Young's modulus, break strength, and elongation at break were obtained from the stress–strain curves.

The morphology of the fracture surface after tensile tests was observed using a Philips XL30 scanning electron microscope (SEM).

Infrared spectra, recorded on a WQF-410 Fourier Transform Infrared (FTIR) spectrometer, were used to investigate the change of epoxy ring before and after curing.

The response of the samples to small-strain mechanical deformation was measured as a function of temperature (−120 to 200°C) using a NETZSCH DMA 242 dynamic mechanical analyzer in a tensile mode. The testing was carried out at a heating rate of 5°C/min in an N_2 atmosphere, frequencies of 1 Hz, a dynamic stress of 5 N, and a static stress of 0.5 N. The sample displacement was 30 μm. Storage moduli (E'), loss moduli (E''), and loss tangent (tan δ) were recorded.

The shape memory properties was tested as following: the sample was cut into 80 × 10 × 0.6 mm strips; then the strips were put into silicone oil at a temperature 20°C higher than the T_g of the sample for 30 min; later the strips were bended around a tube (peripheral curvature, 7.24/dm^{-1}), quenched to room temperature with a constant external force; finally, the shape recovery process of bended strips were observed in silicone oil at a temperature 20°C higher than the T_g of the sample. The shape recovery process was recorded by a camera (SONY, DSC-RX100 M2), and then the video was divided into 25 pictures per second using Corel VideoStudio Pro X4 software. The shape recovery curvature of the strips was determined by bidimensional measurement

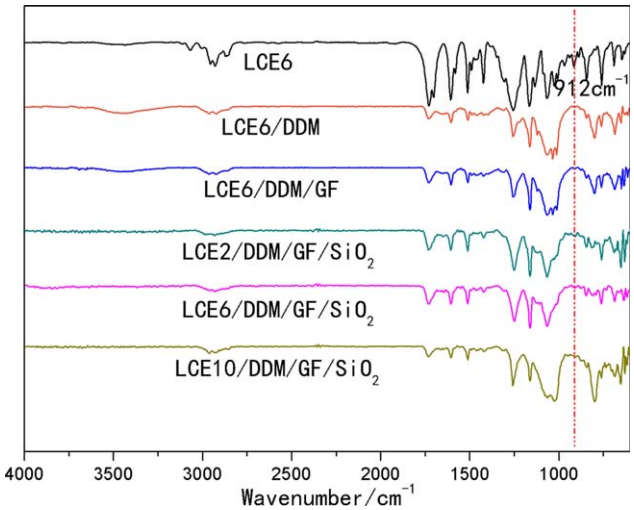

Figure 2. FTIR spectrum of uncured pure LCE6, LCE6/DDM resin and composites. [Color figure can be viewed in the online issue, which is available at wileyonlinelibrary.com.]

software, through which the shape fixing ratio and shape recovery ratio were calculated using the following equations. Repeated to test three samples and selected averages,

$$R_f = (R - R_0)/(R_t - R_0) \quad (1)$$

$$R_r = (R - R')/(R - R_0) \quad (2)$$

where R_f is shape fixed ratio, R_r is shape recovery ratio, R is curvature of the sample after fixing, R_t is curvature of the tube ($7.24/dm^{-1}$), R_0 is curvature of the initial state of the sample, and R' is curvature of the recovered sample.

RESULTS AND DISCUSSION

Curing Degree of the Composite

FTIR spectrums of uncured pure LCE6, LCE6/DDM resin, and LCE/DDM/GF/SiO_2 composites were shown in Figure 2. An absorption peak at 912 cm^{-1} was observed characteristic of the epoxy stretching in the FTIR spectrum of LCE6, while this absorption peak at 912 cm^{-1} could not be found in the spectrums of LCE6/DDM resin, LCE6/DDM/GF composite, and LCE/DDM/GF/SiO_2 composites. These indicated LCE6/DDM resin, LCE6/DDM/GF composite, and LCE/DDM/GF/SiO_2 composites were completely cured and the curing reaction might not be impacted in the presence of glass fibers and nanosilica.

The Liquid Crystalline Phase Structure of LCE and Their Composites

Figure 3 showed the polarized optical microscopic pictures after curing of LCE6/DDM, LCE6/DDM/GF, and nanosilica-modified LCE/DDM/GF composites. Compared POM of LCE6/DDM, LCE6/DDM/GF, and nanosilica-modified LCE/DDM/GF composites, all of them showed common nematic structure with schlieren texture in **LCE2/DDM/GF/SiO_2** composites and the textures were between schlieren and spherulites in LCE6/DDM, LCE6/DDM/GF, and nanosilica-modified LCE6/DDM/GF, and LCE10/DDM/GF composites. Not obvious effect of nanosilica on the phase structure of glass fiber reinforced LCE composites could be observed.

To further investigate the nematic structure affected by nanosilica and lateral substituents, wide-angle X-ray diffraction pattern of LCE6/DDM, LCE6/DDM/GF, and nanosilica-modified LCE/DDM/GF composites were analyzed, as shown in Figure 4. It could be seen that the broad peak around 20° of LCE6/DDM/GF/SiO_2 composites was weaker than that of LCE6/DDM and LCE6/DDM/GF [Figure 4(a)], while broader peaks around 20° of LCE6/DDM/GF/SiO_2 and LCE10/DDM/GF/SiO_2 than LCE2/DDM/GF/SiO_2 composites were observed in Figure 4(b).

It was reported by C.B. McARDLE[28] that the X-ray diffraction patterns of nematic polymers showed, in general, a typical broad peak in the region of $2\theta = 15$–$30°$, classically due to the average lateral distance between the neighboring chains with d-spacing of 3–5 Å. All of the LCE6/DDM, LCE6/DDM/GF, and nanosilica-modified LCE/DDM/GF composites illustrated a typical nematic characteristic with a broad peak around 20° corresponding to d-spacing of 4.3 Å. Curing of liquid crystalline epoxies included linear chain extension at early stage, then branching, and finally cross-linking, which could have significant effects on orientation of mesogenic and structure of liquid crystalline epoxy systems. During linear chain extension stage, the mobility and orientation of mesogen units were hindered by the interactions between nanosilica and liquid crystalline polymer chains.[29] The interactions among nanosilica, mesogen, and lateral substituents acted an obstructed role on orientation of the mesogenic and structure of liquid crystalline epoxy systems. Long alkyl chain substituents could counteract the orientation movement of liquid crystalline polymer chains and the hamper became harder when nanosilica was added, owing to the comprehensive effects of nanosilica and lateral substituents. Thus, LCE6/DDM/GF/SiO_2 composite had lower orientation than

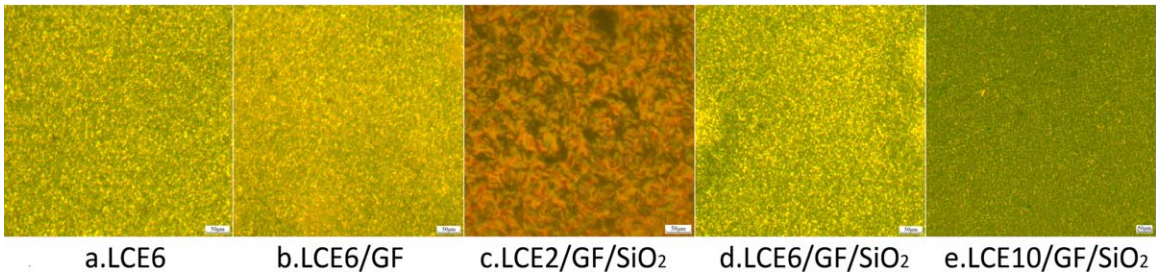

Figure 3. Polarized optical microscopic pictures of LCE6/DDM resin and composites after curing at room temperature. [Color figure can be viewed in the online issue, which is available at wileyonlinelibrary.com.]

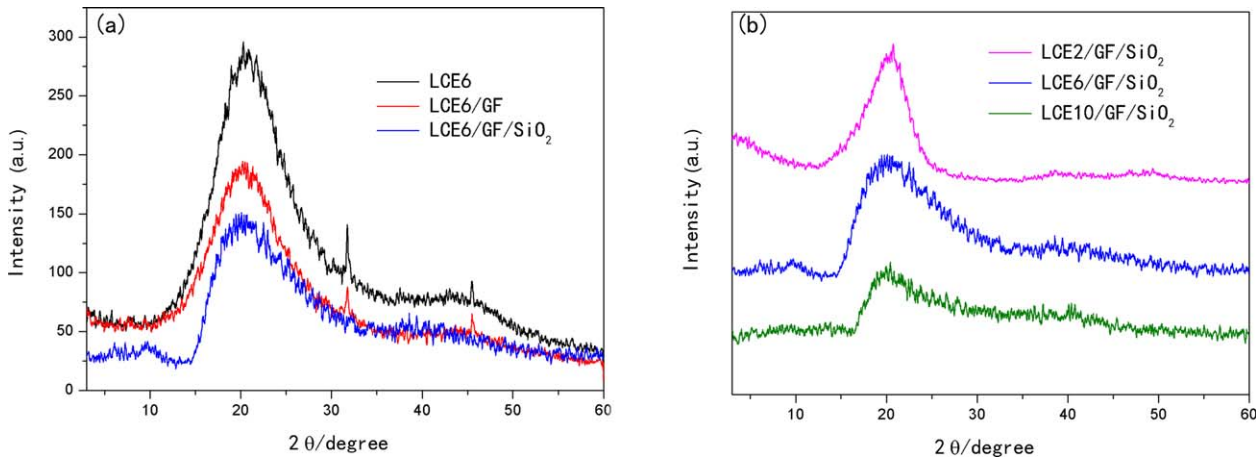

Figure 4. Wide-angle X-ray diffraction measurements of LCE6/DDM resin and composites. [Color figure can be viewed in the online issue, which is available at wileyonlinelibrary.com.]

LCE6/DDM and LCE6/DDM/GF, while LCE2/DDM/GF/SiO_2 composite was more oriented than LCE6/DDM/GF/SiO_2 and LCE10/DDM/GF/SiO_2 composites. Uniaxial oriented nematic structure mode of LCE6/DDM network was shown schematically in Figure 5, from which the effects of nanosilica and lateral substituents on the orientation of mesogenic could be more easily analyzed and understood.

Fracture Morphology and Mechanism

The fracture surface SEMs of LCE6/DDM resin, LCE6/DDM/GF composite, and LCE/DDM/GF/SiO_2 composites were shown in Figure 6. All the test samples for SEM were obtained after tensile test, the fracture surface was treated by spray-gold after being fixed on sample holder. The results showed that both LCE6/DDM resin and LCE6/DDM/GF composite exhibited rough and highly deformed fracture surfaces, while the LCE/DDM/GF/SiO_2 composites illustrated more rough and more highly deformed fracture surfaces with a better interfacial adhesion between LCE6/DDM resin and glass fiber, which were observed in Figure 6(c,d,f). Nanosilica were uniformly dispersed in LCE/DDM resin, shown in Figure 6(e).

It was reported that homogeneous dispersion of nanoparticles in a polymer matrix[19,30–32] could play a beneficial role on the fiber/matrix interfacial adhesion in several types of structural composites. In our work, the uniformly dispersed surface-treated nanosilica within LCE matrix also illustrated a better interfacial adhesion with respect to glass fiber. Good interfacial adhesion between nanoparticle-modified polymer matrix and glass fiber was also observed in some recent reports.[20,22,23,25,26,29,33]

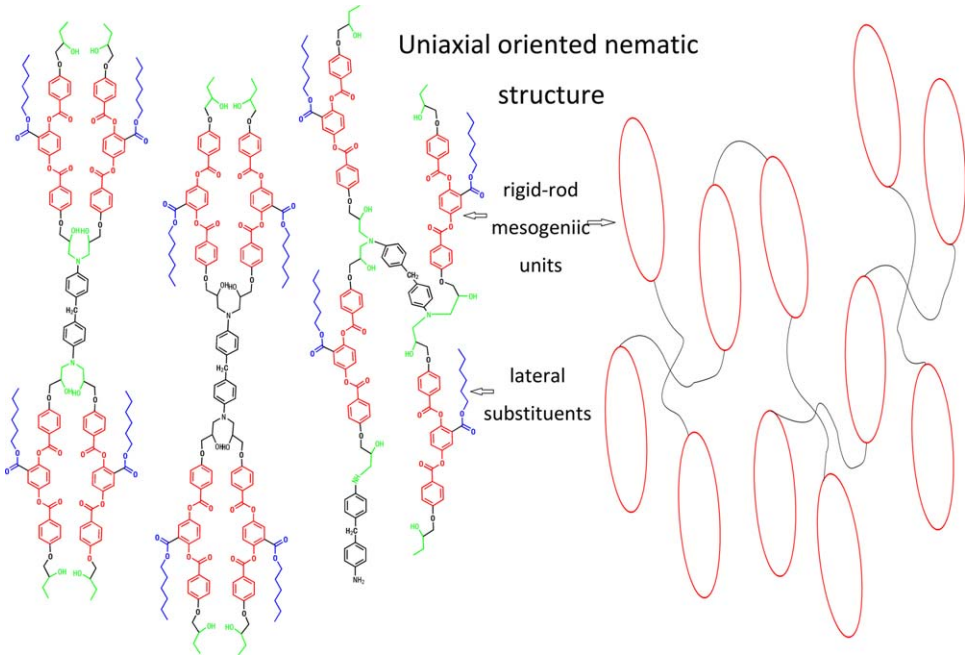

Figure 5. Uniaxial oriented nematic structure mode of LCE6/DDM network. [Color figure can be viewed in the online issue, which is available at wileyonlinelibrary.com.]

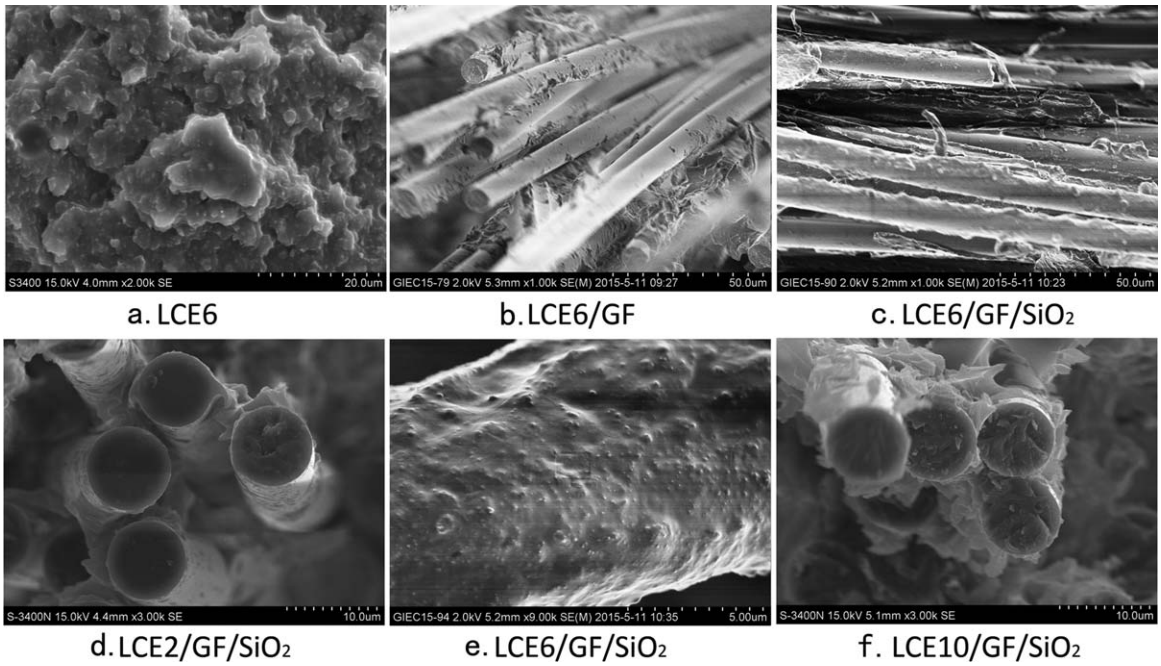

Figure 6. SEM micrographs showing fracture surface of LCE6/DDM resin and composites.

Dynamic Mechanical Analysis

Figure 7 showed the loss tangent (tan δ) data of LCE6/DDM resin, LCE6/DDM/GF composite, and LCE/DDM/GF/SiO_2 composites, from which it could be found that the LCE6/DDM/GF/SiO_2 composite had two peaks, one peak at a temperature similar to LCE6/DDM resin, LCE6/DDM/GF composite, and another peak at a higher temperature [Figure 7(a)], while LCE10/DDM/GF/SiO_2 composite owned two peaks at lower temperature than LCE6/DDM/GF/SiO_2 composite, respectively, nevertheless, LCE2/DDM/GF/SiO_2 composite showed only one peak at a higher temperature than LCE6/DDM/GF/SiO_2 composite [Figure 7(b)], as was illustrated in Table I.

As was well known, T_g or α transition in DMA referred to the temperature at which the network segments began to move. And the movement of network segments could be influenced by the chemical cross-linking, physical entanglement, and the packing density of the segments. As discussed above in Figure 4, the mobility and orientation of mesogen units were hindered in the presence of nanosilica,[29] the branching and cross-linking, served to lock the orientational order permanently into the network,[7,34,35] occurred before achieving well-aligned orientation of mesogen units. Thus, a liquid crystalline phase and an isotropic phase existed in LCE6/DDM/GF/SiO_2 composite compared with LCE6/DDM resin, LCE6/DDM/GF composite. In the liquid

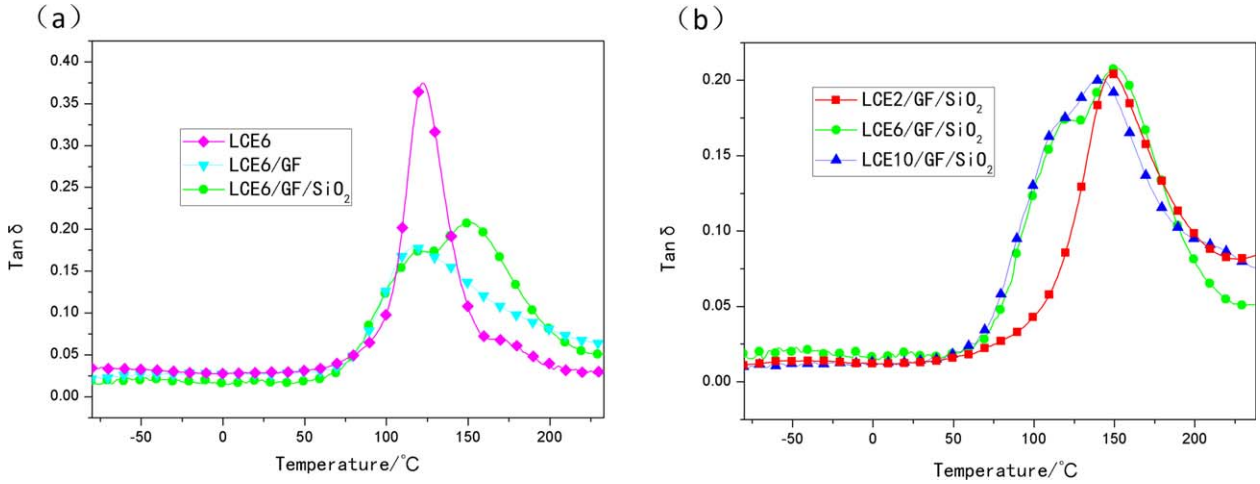

Figure 7. Loss tangent (tan δ) of LCE6/DDM resin and composites. [Color figure can be viewed in the online issue, which is available at wileyonlinelibrary.com.]

Table I. Dynamic Mechanical Results of LCE6/DDM Resin and Composites at 1 Hz

Samples	Storage moduli (E') (MPa) 20°C	Storage moduli (E') (MPa) ($T_g + 20$°C)	T_g (°C)
LCE6	2126	54.54	120
LCE6/GF	6774	1049	117
LCE6/GF/SiO_2	6855	1243/817	119/151
LCE2/GF/SiO_2	7041	1238	148
LCE10/GF/SiO_2	6421	1057/862	116/141

crystalline phase, mainly oriented units were obtained so that the cross-links are mostly chemical in nature. Larger number of physical cross-links were expected to be present in addition to the chemical cross-links in the isotropic phase and extra constraints on the molecular motions were exerted in the isotropic state because of existence of physical cross-links, which caused the shift of the α-transition peak to higher temperatures.[36,37] Therefore, the peak at 119°C is owing to the T_g of the liquid crystalline phase, while the peak at 151°C is due to the T_g of the isotropic phase.

However, the mobility and orientation of mesogen units, though hindered by nanosilica during linear chain extension stage, was easier in LCE2/DDM/GF/SiO_2 composite than in LCE6/DDM/GF/SiO_2 composite and LCE10/DDM/GF/SiO_2 composite, which was attributed to shorter lateral substituents. Thus, a dense and oriented network was obtained in LCE2/DDM/GF/SiO_2 composite. The interchain interactions was stronger in a denser oriented network,[38] that is why only one peak at a higher temperature 148°C was shown in LCE2/DDM/GF/SiO_2 composite, while one liquid crystalline phase T_g at the lowest temperature 116°C and one T_g of the liquid crystalline phase at a lower temperature 119°C were observed in the LCE10/DDM/GF/SiO_2 composite and LCE6/DDM/GF/SiO_2 composite, respectively [Figure 6(b)], owing to longer lateral substituent.

The dynamic storage moduli (E') and dynamic loss moduli (E'') of LCE6/DDM resin, LCE6/DDM/GF composite, and LCE/DDM/GF/SiO_2 composites were shown in Figures 8 and 9. All of them show a broad peak centered at about −50°C and a strong peak in the E'' curve. In correspondence with the first broad peaks, E' is slightly reduced, while it drops after the second strong peak, for LCE6/DDM resin, LCE6/DDM/GF composite, and LCE/DDM/GF/SiO_2 composites. The strong peak was attributed to T_g or α transition in DMA, as was discussed above.

The broad peaks corresponded to the β transition which could also be seen in the loss tangent (tan δ) data of LCE6/DDM resin, LCE6/DDM/GF composite, and LCE/DDM/GF/SiO_2 composites (Figure 7), originating from the small-scale motion of polymer networks, which included the movements of side chains or pendent groups.[39] The β transition temperature showed no significant difference among LCE6/DDM resin, LCE6/DDM/GF composite, and LCE/DDM/GF/SiO_2 composites. It could be explained that the distance between mesogenic units was almost the same for LCE6/DDM resin, LCE6/DDM/GF composite, and LCE/DDM/GF/SiO_2 composites (It could be seen in Figure 3 that the nematic intense diffraction peaks were at around 20° with d-spacing of 4.3 Å for all the samples.).

From Figure 8, it could be found that the dynamic storage moduli (E') of the LCE6/DDM/GF/SiO_2 composite was about 3 times higher than that of the LCE6/DDM resin. The dynamic storage moduli (E') of the LCE6/DDM/GF/SiO_2 composite at 20°C was 6.9 GPa (higher than that of LCE6/DDM/GF composite), while the E' of LCE6/DDM resin at 20°C was only 2.1 GPa, as was illustrated in Table I. As was discussed above, the surface-treated nanosilica could improve interfacial adhesion with respect to glass fiber (Figure 6), so that the dynamic storage moduli (E') of the LCE6/DDM/GF/SiO_2 composite were higher than that of the LCE6/DDM/GF composite. And it could also be found that the storage modulus decreased with the length of lateral substituents, which was likely because the long lateral substituents decreased the rigidity of mesogenic core and lead to mesogens oriented easily in the direction of applied stress.[38]

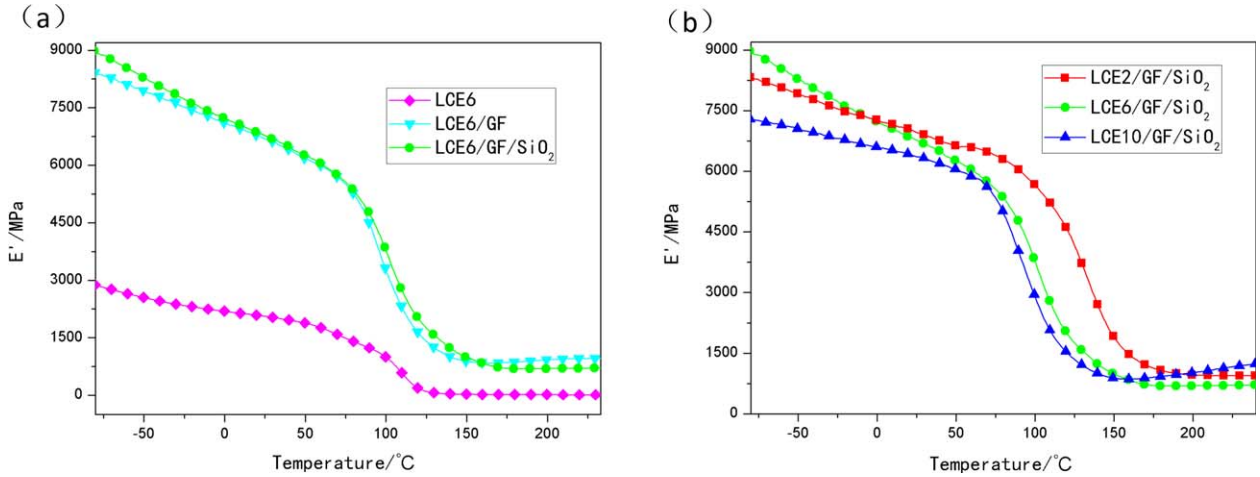

Figure 8. Dynamic storage moduli (E') of LCE6/DDM resin and composites. [Color figure can be viewed in the online issue, which is available at wileyonlinelibrary.com.]

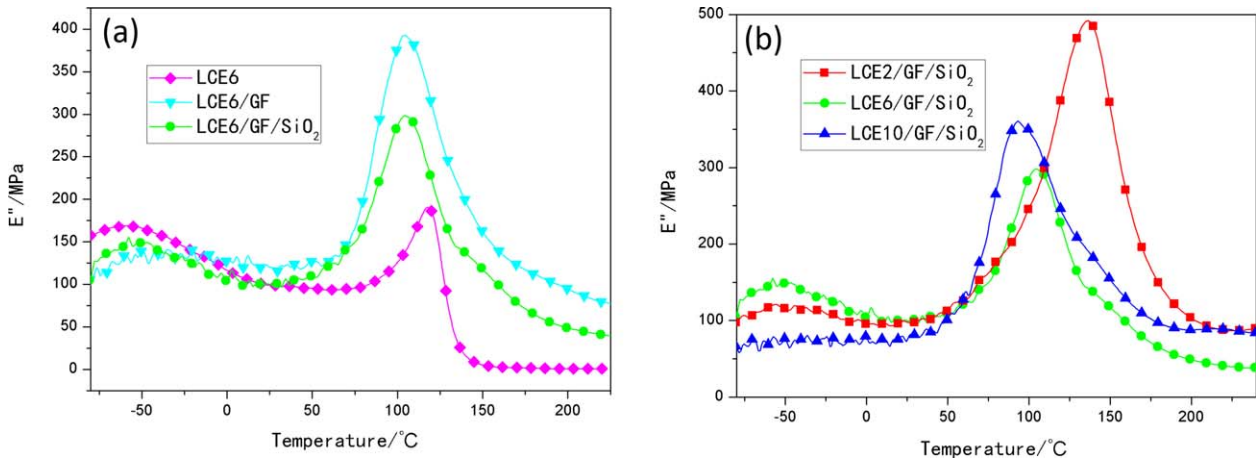

Figure 9. Dynamic loss moduli (E'') of LCE6/DDM resin and composites. [Color figure can be viewed in the online issue, which is available at wileyonlinelibrary.com.]

Mechanical Properties

Figure 10 showed the relationships between the tensile stresses versus strain at room temperature and 150°C. It was observed from Figure 10(a,c) that the modulus and the tensile strength of LCE6/DDM/GF/SiO_2 composite at room temperature were nearly 3 times higher than LCE6/DDM resin, slightly higher than LCE6/DDM/GF composite. Moreover, the modulus and the tensile strength of LCE6/DDM/GF/SiO_2 composite at 150°C were extremely higher than LCE6/DDM resin, while the elongation at break of LCE6/DDM/GF/SiO_2 composite was the lowest compared with LCE6/DDM resin and LCE6/DDM/GF composite at room temperature or 150°C, and the elongation at break

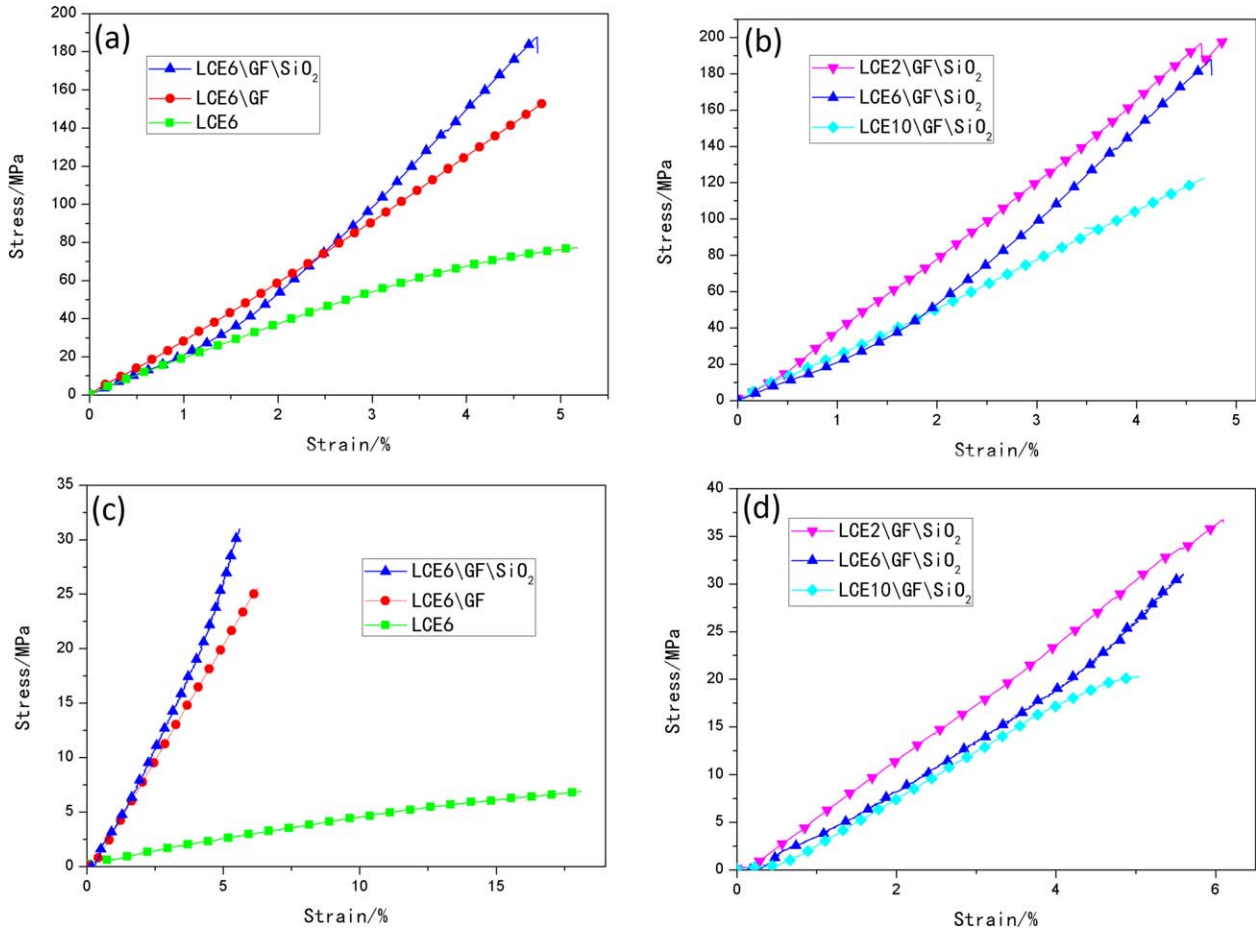

Figure 10. Stress versus strain curves for LCE6/DDM resin and composites at room temperature and 150°C. [Color figure can be viewed in the online issue, which is available at wileyonlinelibrary.com.]

Table II. Tensile Results of LCE6/DDM Resin and Composites at Room Temperature and 150°C

	E (MPa)		ε_b (%)		δ_b (MPa)	
Sample	25°C	150°C	25°C	150°C	25°C	150°C
LCE6	1778	40	5.17	18.12	61.85	6.91
LCE6/GF	3186	538	4.82	6.29	153.57	25.58
LCE6/GF/SiO_2	3780	584	4.75	5.59	179.36	30.99
LCE2/GF/SiO_2	4083	598	4.89	6.10	199.73	36.47
LCE10/GF/SiO_2	2617	403	4.68	5.04	122.46	20.27

of LCE6/DDM resin at 150°C reached up to 18%, as was illustrated in Table II.

As was well known, glass fiber, as reinforcing fillers, could greatly improve the mechanical properties of the polymer matrix. It was reported in the review of Shao-Yun Fu *et al.*[40] the mechanical properties of polymers could be modified by inorganic particulate fillers. Peerapan Dittanet *et al.*[41] confirmed that the Young's modulus was significantly improved with addition of silica nanoparticles into epoxy matrix. It was confirmed by Zhen Li *et al.*[42] that the tensile strength of liquid crystalline networks at high temperature was enhanced when the SiO_2 nanoparticles were added. Other reports[19,20,24] confirmed that nanosilica could modify the intrinsic defects on the surfaces of GFs, so that the mechanical performances of glass-fiber-reinforced polymer composites could be improved by importing a small amount of nanosilica into the polymer matrix. From SEM, it could be found that a better interfacial adhesion existed between LCE6/DDM resin and glass fiber (Figure 6). Three failure modes existed in fiber-enhanced polymer composite: (a) fiber breakage/rupture; (b) debonding between interfacial coating layer and polymer matrix; (c) debonding at fiber/polymer matrix interface.[43] The better interfacial adhesion caused by nanosilica made the failure modes change from debonding at fiber/polymer matrix interface to debonding between interfacial coating layer and polymer matrix. And debonding between interfacial coating layer and polymer matrix caused the failure be rather determined by the fracture of glass fiber than LCE6/DDM matrix. Therefore, the LCE6/DDM/GF/SiO_2 composite had the highest modulus, highest tensile strength, and lowest elongation at break than LCE6/DDM resin and LCE6/DDM/GF composite, owing to much higher modulus and tensile strength and much lower elongation at break of glass fiber compared to LCEs. In addition, the effect of temperature on the mechanical properties of glass fiber was not as LCE so obvious, so that the elongation at break of LCE6/DDM resin at 150°C reached up to 18% which was almost three times longer than LCE6/DDM/GF composite and LCE6/DDM/GF/SiO_2 composite. The network segments of LCE6/DDM resin could move easily at 150°C, which was in its rubbery region, resulting in lower modulus and tensile strength.

It was also found that the modulus, strength at break, and elongation of LCE decrease with the length increase of lateral substituents at room temperature or 150°C (Figure 10(b,d) and Table II). This was due to decreased density of network and the easily oriented mesogens in the direction of external force which was caused by large lateral substituents.[38]

Shape Memory Properties Analysis

The shape recovery process and the shape recovery curvature of the strips were shown in Figures 11 and 12. Table III illustrated the shape fixing ratio and shape recovery ratio of LCE6/DDM resin, LCE6/DDM/GF composite, and LCE/DDM/GF/SiO_2 composites. It could be found that the shape recovery speed and the shape fixing ratio (98%) of the LCE6/DDM resin was the highest and that decreased with the addition of glass fiber. The LCE6/DDM/GF/SiO_2 composite showed a higher shape recovery speed and shape fixing ratio, compared with LCE6/DDM/GF composite. While as the increase of the length of the lateral substituents, the shape recovery speed decreased in the LCE/DDM/GF/SiO_2 composites. All the samples could be almost completely recovered with shape recovery ratios higher than 98%.

There was an oriented and chemically cross-linked structure in liquid crystalline epoxides (LCEs). The oriented mesogen and chemically cross-linked network made LCE6/DDM resin an excellent shape memory material, with higher shape fixing ratio (98%) and shape recovery ratio (98.6%) and extremely fast shape recovery process within 4 s. This indicated that this liquid crystalline epoxy could be a preferred candidate for shape memory composites matrix. This shape memory effect is driven by the entropic behavior in the aromatic ester mesogenics between the cross-links of LCEs. Below T_g, the aromatic ester mesogenics between the network points could not change any conformation and were locked into the orientational order network permanently unless a suitably large mechanical force was applied. The rotational conformations of aromatic ester mesogenics could be changed at relatively lower stresses when heated above T_g. Above T_g, the aromatic ester mesogenics could be aligned in the direction of stresses, increasing the stored energy in LCEs as the entropy of the LCE chains decreased. Upon cooling in the deformed shape, the LCE chains could no longer freely rotate. The aromatic ester mesogenics then recovered this stored energy by returning to the initial high entropy configuration when the samples were heated above T_g. **It was clear that glass fabric played an obstructive role on the shape memory effect of the composites, while the influence of nanosilica on the shape memory effect of the composites was quite complicated. As was discussed in the section titled "The Liquid Crystalline Phase Structure of LCE and Their Composites,"** the mobility and orientation of mesogen units were hindered by the

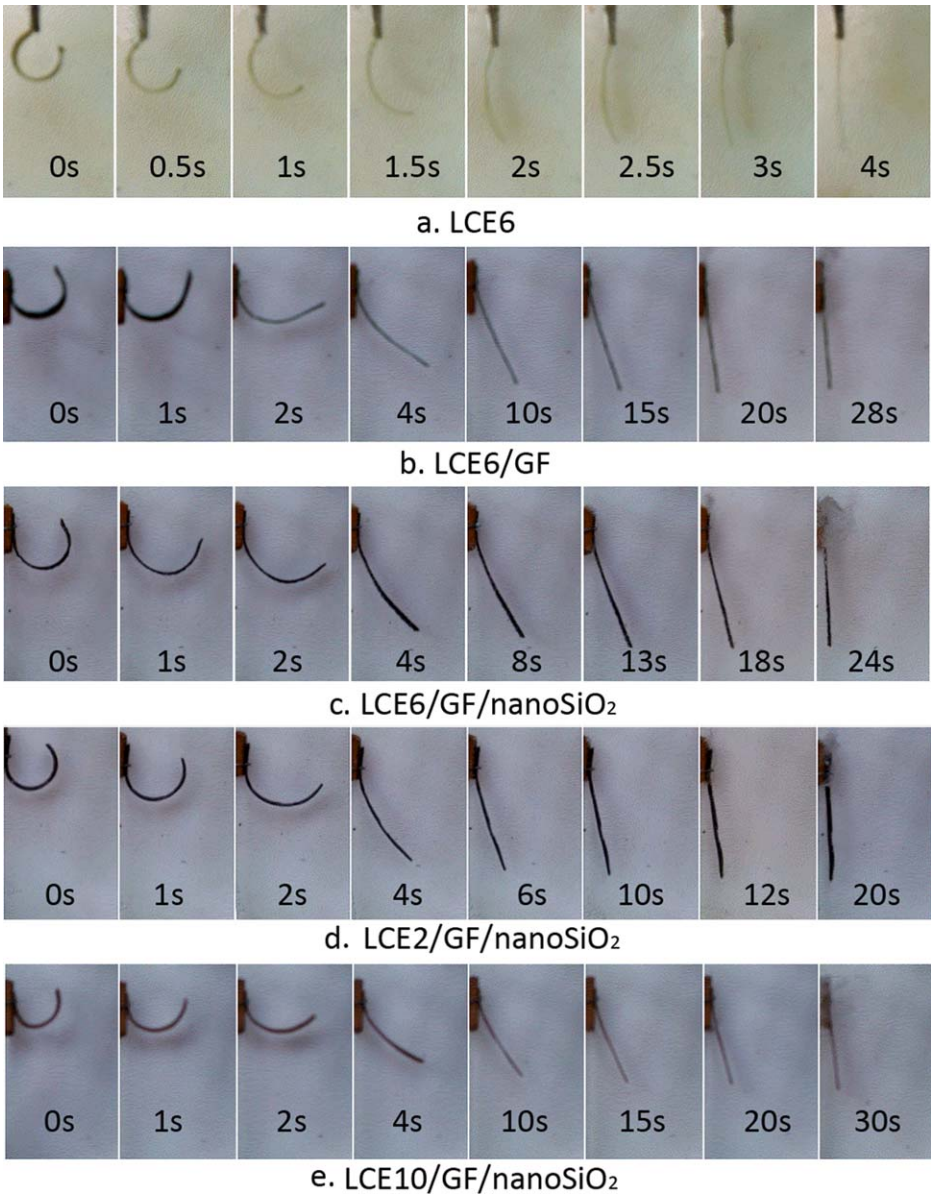

Figure 11. Shape recovery process pictures for LCE6/DDM resin and composites. [Color figure can be viewed in the online issue, which is available at wileyonlinelibrary.com.]

interactions between nanosilica and liquid crystalline polymer chains. **During the shape memory experiment, shape memory effect was also obstructed owing to the obstructive movement of aromatic ester mesogenics caused by the nanosilica. However, larger number of physical cross-links was present in LCE6/DDM/GF/SiO_2 composite than in LCE6/DDM/GF composite with similar chemical cross-links in both composites, as was discussed in the section titled "Dynamic Mechanical Analysis". And** the cross-link structure played a crucial role **on the shape memory effect. Therefore,** in the LCE6/DDM/GF composite, the LCE network should overcome the obstruction of glass fabric during shape fixing and shape recovery process, resulting in decreased shape fixing ratio of and shape recovery speed of LCE6/DDM/GF composite. Whereas higher shape fixing ratio of LCE6/DDM/GF/SiO_2 composite than that of LCE6/DDM/GF composite was caused by the present of larger number of physical cross-links in LCE6/DDM/GF/SiO_2 composite than that in LCE6/DDM/GF composite with similar chemical cross-links in both composites. The storage moduli at temperature 20°C higher than T_g of LCE6/DDM/GF/SiO_2 composite and the tensile moduli of LCE6/DDM/GF/SiO_2 composite at 150°C were higher than that of LCE6/DDM/GF composite, and then the shape recovery stress of LCE6/DDM/GF/SiO_2 composite was expected to be higher than that of LCE6/DDM/GF composite, therefore, the shape recovery process was accelerated with the addition of surface-treated nanosilica. The shape recovery ratio, on behalf of the ability of returning to their original state of shape memory epoxies, was dominated by the LCE resin in our work, resulting in little change in the shape recovery ratios of LCE6/DDM resin, LCE6/DDM/GF composite, and LCE6/DDM/GF/SiO_2 composite.

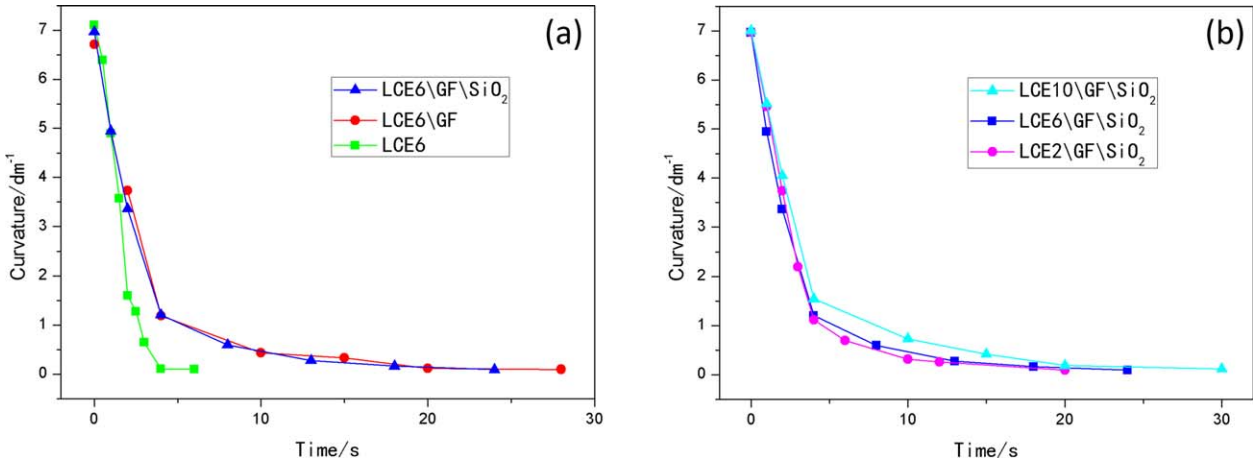

Figure 12. Shape recovery curvature versus time for LCE6/DDM resin and composites. [Color figure can be viewed in the online issue, which is available at wileyonlinelibrary.com.]

As was reported by our group,[38,44] the cross-linking density of LCE network decreased with increase of the length of the lateral substituents. The cross-linking density of LCE network acted an important role in shape memory effects. That is why the shape recovery speeds of LCE/DDM/GF/SiO_2 composites decreased as the length of lateral substituents increased, which was consistent with our previous work.[17,18]

CONCLUSIONS

Thermoresponsive shape memory composites with enhanced mechanical properties based on glass fiber and nanosilica-modified LCE with lateral substituent were prepared and characterized in this study. The composites could recover to their original state quickly in a time shorter than 30 s with high shape fixing ratios (>96%) and high shape recovery ratios (>98%), owing to additional physical cross-links and higher shape recovery stress induced by the introduction of surface-treated nanosilica, which indicated the composites could be applied into self-deploying structural materials. Moreover, the reinforcement in the dynamic storage moduli, tensile modulus, and the tensile strength and shape memory properties indicated that these LCE/DDM/GF/SiO_2 composites could be high-performance composites and could be used as new candidates for aerospace smart materials.

The orientation of mesogen units were hindered by the introduction of nanosilica and lateral substituents of liquid crystalline epoxies, so that additional physical cross-links except for similar chemical cross-links emerged with the introduction of surface-treated nanosilica, according to the comprehensive analysis of polarized optical microscopy, wide-angle X-ray diffraction measurements, and tan δ data. The increased cross-links which dominate the netponts determining the permanent shape of shape memory polymers acted a positive role in the shape memory effect of the nanosilica-modified LCE composites.

The fracture surface SEM micrographs showed that the composites illustrated more rough and more highly deformed fracture surfaces with a better interfacial adhesion between LCE6/DDM resin and glass fiber, so that the dynamic storage moduli, tensile modulus, the tensile strength, and shape memory properties (shape fixing ratio >96%, shape recovery ratio >98%, and shape recovery time <24 s) were improved in the glass fiber and nanosilica-modified LCE with lateral substituent composite. However, the elongation at break decreased slightly with the addition of nanosilica, while the elongation at break of LCE6/DDM resin at 150°C was over three times than the composites.

While in the LCE/DDM/GF/SiO_2 composites the glass transition temperature, thermal stability, dynamic storage moduli, tensile modulus, the tensile strength, elongation at break, and shape recovery speeds (shape recovery time <30 s) decreased with increase of the length of lateral substituents.

Table III. Shape Fixing Ratio and Shape Recovery Ratio of LCE6/DDM Resin and Composites

Sample	R_f (%)	R_r (%)
LCE6	98.1	98.6
LCE6/GF	92.8	98.5
LCE6/GF/SiO_2	96.1	98.6
LCE2/GF/SiO_2	96.2	98.6
LCE10/GF/SiO_2	96.3	98.3

ACKNOWLEDGMENTS

This research was supported by the intergration of Industry Education and Research of Guangdong Province project (2011A091000007) and the National Natural Science Foundation of China (20974121).

REFERENCES

1. Meng, Q. H.; Hu, J. L. *Compos. Part A: Appl. Sci.* **2009**, *40*, 1661.
2. Meng, H.; Li, G. Q. *Polymer* **2013**, *54*, 2199.
3. Wei, K.; Zhu, G.; Tang, Y.; Li, X.; Liu, T.; Niu, L. *Compos. Part B: Eng.* **2013**, *51*, 169.
4. Kumar, K. S. S.; Biju, R.; Nair, C. P. R. *React. Funct. Polym.* **2013**, *73*, 421.

5. Wu, X. L.; Kang, S. F.; Xu, X. J.; Xiao, F.; Ge, X. L. *J. Appl. Polym. Sci.* **2014**, *131*, DOI: 10.1002/app.40559.
6. Carfagna, C.; Amendola, E.; Giamberini, M. *Compos. Struct.* **1994**, *27*, 37.
7. Barclay, G. G.; Ober, C. K. *Prog. Polym. Sci.* **1993**, *18*, 899.
8. Guo, H.; Lu, M.; Liang, L.; Zheng, J.; Zhang, Y.; Li, Y.; Li, Z.; Yang, C. *J. Appl. Polym. Sci.* **2014**, *131*, DOI: 10.1002/app.40363.
9. Lee, J. Y.; Jang, J. *Polym. Bull.* **2007**, *59*, 261.
10. Wei, K.; Zhu, G.; Tang, Y.; Liu, T.; Xie, J. *J. Mater. Res.* **2013**, *28*, 2903.
11. Liu, Y.; Sun, H.; Tan, H.; Du, X. *J. Appl. Polym. Sci.* **2013**, *127*, 3152.
12. Song, W. B.; Wang, L. Y.; Wang, Z. D. *Mat. Sci. Eng. A Struct.* **2011**, *529*, 29.
13. Leonardi, A. B.; Fasce, L. A.; Zucchi, I. A.; Hoppe, C. E.; Soule, E. R.; Perez, C. J.; Williams, R. J. *J. Eur. Polym. J.* **2011**, *47*, 362.
14. Xie, T.; Rousseau, I. A. *Polymer* **2009**, *50*, 1852.
15. Dong, Y.; Ni, Q.-Q.; Li, L.; Fu, Y. *Mater. Lett.* **2014**, *132*, 206.
16. Dong, Y.; Ding, J.; Wang, J.; Fu, X.; Hu, H.; Li, S.; Yang, H.; Xu, C.; Du, M.; Fu, Y. *Compos. Sci. Technol.* **2013**, *76*, 8.
17. Shen, T.; Wu, F.; Sun, C. *J. Macromol. Sci. A* **2013**, *50*, 1085.
18. Liang, L.; Zhou, D.; Lu, M. Study on shape memory effects of LC epoxy resins with lateral substituents, In International Symposium on Liquid Crystal Science and Technology, Huang, Y.M., Ed., Kunming, **2010**, *391*.
19. Pedrazzoli, D.; Pegoretti, A. *Compos. Sci. Technol.* **2013**, *76*, 77.
20. Manjunatha, C. M.; Taylor, A. C.; Kinloch, A. J.; Sprenger, S. *Compos. Sci. Technol.* **2010**, *70*, 193.
21. Liu, Y.; Xiao, H.-M.; Feng, Q.-P.; Fu, S.-Y. *Compos. Part A-Appl. Sci.* **2014**, *62*, 39.
22. Nguyen, Q.; Ngo, T.; Moinuddin, K.; Mendis, P. Use of nanoclay to improve fire performance of glass fibre composites, Fourth International Conference on Smart Materials and Nanotechnology in Engineering, Gold Coast, Australia, **2013**, 8793
23. Cao, Y.; Cameron, J. *J. Reinf. Plast. Compos.* **2006**, *25*, 761.
24. Boeger, L.; Sumfleth, J.; Hedemann, H.; Schulte, K. *Compos. Part A: Appl. Sci.* **2010**, *41*, 1419.
25. Cao, Y.; Cameron, J. *J. Reinf. Plast. Compos.* **2006**, *25*, 347.
26. Sprenger, S. *J. Mater. Sci.* **2014**, *49*, 2391.
27. Zheng, Y.; Shen, M.; Lu, M.; Ren, S. *Eur. Polym. J.* **2006**, *42*, 1735.
28. Mcardle, C. B. Side Chain Liquid Crystal Polymers; Chapman and Hall: New York, NY, **1989**; Chapter 6.
29. Giamberini, M.; Malucelli, G. *Thin Solid Films* **2013**, *548*, 150.
30. Vlasveld, D. P. N.; Parlevliet, P. P.; Bersee, H. E. N.; Picken, S. *J. Compos. Part A-Appl. Sci.* **2005**, *36*, 1.
31. Zhamu, A.; Zhong, W. H.; Stone, J. J. *Compos. Sci. Technol.* **2006**, *66*, 2736.
32. Dorigato, A.; Morandi, S.; Pegoretti, A. *J. Compos. Mater.* **2012**, *46*, 1439.
33. Manjunatha, C. M.; Bojja, R.; Jagannathan, N.; Kinloch, A. J.; Taylor, A. C. *Int. J. Fatigue* **2013**, *54*, 25.
34. Giamberini, M.; Amendola, E.; Carfagna, C. *Mol. Cryst. Liq. Crys. A* **1995**, *266*, 9.
35. Shiota, A.; Ober, C. K. *Prog. Polym. Sci.* **1997**, *22*, 975.
36. Giamberini, M.; Malucelli, G.; Ambrogi, V.; Capitani, D.; Cerruti, P. *Polym. Int.* **2010**, *59*, 1415.
37. Sue, H. J.; Earls, J. D.; Hefner, R. E. *J. Mater. Sci.* **1997**, *32*, 4031.
38. Zheng, Y.; Lu, M.; Ren, S.; Hang, L.; Lan, Y. *J. Polym. Sci. Part B: Polym. Phys.* **2007**, *45*, 2835.
39. Tan, C. B.; Sun, H.; Fung, B. M.; Grady, B. P. *Macromolecules* **2000**, *33*, 6249.
40. Fu, S. Y.; Feng, X. Q.; Lauke, B.; Mai, Y. W. *Compos. Part B Eng.* **2008**, *39*, 933.
41. Dittanet, P.; Pearson, R. A. *Polymer* **2012**, *53*, 1890.
42. Li, Z.; Yang, Y.; Qin, B.; Zhang, X.; Tao, L.; Wei, Y.; Ji, Y. *Materials* **2014**, *7*, 5356.
43. Ning, N.; Fu, S.; Zhang, W.; Chen, F.; Wang, K.; Deng, H.; Zhang, Q.; Fu, Q. *Prog. Polym. Sci.* **2012**, *37*, 1425.
44. Liang, L.; Ren, S.; Zheng, Y.; Lan, Y.; Lu, M. *Polym. J.* **2007**, *39*, 961.